TITLE:

In Situ Surface Roughness Analysis of Electrodeposited Co Films in an Ionic Liquid Using Electrochemical Surface Plasmon Resonance: Effect of Leveling Additives

AUTHOR(S):

Nishi, Naoya; Ezawa, Kenta; Sakka, Tetsuo

CITATION:

Nishi, Naoya ...[et al]. In Situ Surface Roughness Analysis of Electrodeposited Co Films in an Ionic Liquid Using Electrochemical Surface Plasmon Resonance: Effect of Leveling Additives. Journal of the Electrochemical Society 2021, 168(7): 072505.

ISSUE DATE:

2021-07

URL:

http://hdl.handle.net/2433/265475

RIGHT:

This is the Accepted Manuscript version of an article accepted for publication in Journal of The Electrochemical Society. The Electrochemical Society and IOP Publishing Ltd are not responsible for any errors or omissions in this version of the manuscript or any version derived from it. The Version of Record is available online at https://doi.org/10.1149/1945-7111/ac13d1.; This is not the published version. Please cite only the published version. この論文は出版社版でありません。引用の際には出版社版をご確認ご利用ください。

京都大学学術情報リポジトリ
KURENAI 紅
Kyoto University Research Information Repository

京都大学 KYOTO UNIVERSITY
A Self-archived copy in
Kyoto University Research Information Repository
https://repository.kulib.kyoto-u.ac.jp
京都大学学術情報リポジトリ KURENAI 紅 Kyoto University Research Information Repository

In-situ surface roughness analysis of electrodeposited Co films in an ionic liquid using electrochemical surface plasmon resonance: effect of leveling additives

Naoya Nishi,* Kenta Ezawa, and Tetsuo Sakka

Department of Energy and Hydrocarbon Chemistry, Graduate School of Engineering, Kyoto University, Kyoto, 615-8510, Japan

nishi.naoya.7e@kyoto-u.ac.jp

Abstract

The effect of two leveling additives, thiourea (TU) and coumarin (CM), on cobalt electrodeposition process in an ionic liquid (IL), 1-butyl-3-methylimidazolium bis(trifluoromethanesulfonyl)amide (C4mimTFSA), at the gold surface has been analyzed in-situ using electrochemical surface plasmon resonance (ESPR), in which the SPR resonance angle (Δθ) has been recorded simultaneously with cyclic voltammograms. The two additives show Δθ behaviors different from the additive-free case and from each other. In the case of TU, the positive Δθ shift due to Co cathodic deposition is larger than the additive-free case. Even after the subsequent negative Δθ shift due to Co anodic dissolution, Δθ remains positive not returning to the original value. This indicates that the dissolution of gold facilitated by TU roughens the surface of the gold electrode. In contrast, in the case of CM, the positive Δθ shift due to

京都大学 KYOTO UNIVERSITY
A Self-archived copy in
Kyoto University Research Information Repository
https://repository.kulib.kyoto-u.ac.jp
京都大学学術情報リポジトリ KURENAI 紅 Kyoto University Research Information Repository

Co cathodic deposition is smaller than the additive-free case. A model analysis using Fresnel reflectivity has revealed that CM actually smooths the surface of the Co film even in the initial process of the electrodeposition. These findings illustrate that ESPR can sense in-situ the surface roughness change during electrodeposition on the order of Å.

KEYWORDS: Ionic liquid/gold interface; NTf_2; leveler

京都大学 KYOTO UNIVERSITY
A Self-archived copy in
Kyoto University Research Information Repository
https://repository.kulib.kyoto-u.ac.jp
京都大学学術情報リポジトリ KURENAI 紅 Kyoto University Research Information Repository

1. Introduction

Ionic liquids (ILs), low-temperature molten salts entirely composed of cations and anions, have characteristics such as wide potential window and high stability over a wide temperature range. Due to these characteristics, ILs have been promising materials as electrolytes for metal anode secondary batteries [1,2] and metal plating [3,4] where metal electrodeposition on the electrode is a critical process. Electrodeposition in ILs has been extensively studied in a wide range of metal elements not only noble metals but also base metals by virtue of the wide potential window.

Co is one of the most important base metals constituting magnetic and corrosion-resistant alloys. The electrodeposition of Co and its alloys in ILs has been actively studied [5–14][15–24][25]. The Co electrodeposition in ILs is known to show a high activation overpotential. Katayama et al. suggested that a complex anion of Co^{2+} in ILs (e.g., $[Co(TFSA)_3]^{-}$, where $TFSA^{-}$ is bis(trifluoromethanesulfonyl)amide) encounters a large activation barrier when crossing the cation-rich ionic layer on the electrode to approach the electrode surface during the cathodic deposition in which the electrode potential is negatively charged [20,22]. The activation overpotential decreased when leveling additives, acetone (AC) [20] or thiourea (TU) [22], were added. The decrease is likely to result from the formation of a complex cation ($[Co(AC)_4]^{2+}$ or $[Co(TU)_4]^{2+}$), which can be located in the surface cationic layer on the electrode [20,22]. The surface of the deposited Co film became smoother, confirmed by ex-situ SEM [22]. An EQCM study by Tułodziecki et al. [23] and a SEIRAS study by Motobayashi et al. [25] studied the Co electrodeposition in ILs with and without TU, and both confirmed that the high activation overpotential originates from the slow structural dynamics in the surface ionic layers, which is inherent to ILs [26,27].

京都大学 KYOTO UNIVERSITY
A Self-archived copy in
Kyoto University Research Information Repository
https://repository.kulib.kyoto-u.ac.jp
京都大学学術情報リポジトリ KURENAI 紅 Kyoto University Research Information Repository

There are various leveling additives other than AC and TU, such as p-toluenesulfonamide [28], saccharin [29], and coumarin (CM) that reduce the deposition overpotential and smooth the deposited film surface. CM has been used for the electrodeposition of Co [22] and Ni [28,30,31]. Regarding the leveling mechanism, CM is decomposed and depleted at microscopically concave parts of the electrode surface, where metal electrodeposition preferentially occurs [31,32]. CM was found to smooth the surface of the electrodeposited film and reduced the activation overpotential in Co electrodeposition in ILs [22].

For ex-situ analysis of Co and Co-alloy films electrodeposited in ILs, several methods have been used such as SEM [6,7,9,11,17,19–21,23,24] (with EDX) and XRD [7–9,11,19,21]. In contrast, for in-situ analysis of the electrodeposited Co film surface in ILs, only a few methods have been reported such as STM/STS [14,15,18]. In the present study, we propose electrochemical surface plasmon resonance (ESPR) as one of the in-situ analysis methods for the surface roughness of electrodeposited films. Previously we applied ESPR to reveal electrochemical processes at the electrode interface of ILs in an in-situ manner and found that ESPR can sensitively detect the change in the interfacial structure such as the ionic composition in the electric double layer (EDL) [27,33] and the diffusion layer of dissolved redox species [34,35]. In a recent paper, we studied the electrodeposition process of Cu using ESPR in an IL, 1-butyl-3-methylimidazolium bis(trifluoromethanesulfonyl)amide (C_4mimTFSA), and found that repeated cathodic deposition/anodic dissolution of Cu results in the smoothing of the gold electrode surface with a Å resolution [35]. However, it has been unclear whether or not this surface smoothing is a ubiquitous phenomenon during metal electrodeposition in general. Moreover, despite its high sensitivity on the surface roughness, ESPR has not

京都大学 KYOTO UNIVERSITY
A Self-archived copy in
Kyoto University Research Information Repository
https://repository.kulib.kyoto-u.ac.jp
京都大学学術情報リポジトリ KURENAI 紅 Kyoto University Research Information Repository

been used to explore how leveling additives affect the surface roughness during the electrodeposition. In the present study, we will present ESPR measurements for the initial stage of the Co electrodeposition process on the gold electrode in C_4mimTFSA, focusing on the leveling additive effect on the surface roughness of both the gold electrode and electrodeposited Co film. Our in-situ ESPR analysis, combined with ex-situ AFM, and CV and Fresnel reflectivity simulations, revealed that the surface roughnesses during the Co electrodeposition process vary depending on the presence/absence of leveling additives and also their kinds.

2. Experimental

2-1. Reagent

Cobalt bis(trifluoromethanesulfonyl)amide ($Co(TFSA)_2$) was obtained by adding $CoCO_3$ (Kanto Chemical) to a 70 wt% HTFSA aqueous solution (Central Glass) until the solution showed pH≅7 followed by water removal using an evaporator. $Co(TFSA)_2$ was dissolved into C_4mimTFSA (synthesized [35]) at a concentration of 5 mM. TU (Wako) and CM (TCI), which are leveling additives, were dissolved to the Co-containing IL so that the formal concentrations were 20, 5, and 1.25 mM for TU and 5 mM for CM.

2-2. Electrochemical Surface Plasmon Resonance (ESPR)

京都大学 KYOTO UNIVERSITY
A Self-archived copy in
Kyoto University Research Information Repository
https://repository.kulib.kyoto-u.ac.jp
京都大学学術情報リポジトリ KURENAI 紅 Kyoto University Research Information Repository

SPRINGLE (KEI) was used for the ESPR measurements, the details of which were described in our previous studies [33,35]. The working electrode was a gold film (50 nm thickness, 0.071 cm^2 surface area) coated on an SF15 glass substrate, the counter electrode was Pt, and the pseudo-reference electrode was a Ag/AgCl wire. The SPR angle shift ($\Delta\theta$) at 670 nm was recorded simultaneously with multi-scan cyclic voltammograms with a scan rate of 50 mV s^{-1} in Ar atmosphere at room temperature. Before each CV scan, the potential was held at the starting potential for 2000 s to equilibrate the EDL structure [27,33,36]. The $\Delta\theta$ values were set to $\Delta\theta = 0$ at the beginning of each scan.

2-3. Ex-situ atomic force microscope (AFM) observation of gold surface

The surface of the gold electrode was observed ex-situ (in air) before and after the ESPR measurements using an atomic force microscope (SPM-9600, Shimadzu) [35]. The root mean square of the surface height variation, R_q, was calculated from the height data of AFM images and the surface roughness, d_0, was estimated using a relation $d_0 = (1.175 \pm 0.285)R_\mathrm{q}$ [37,38].

2-4. Simulation of resonance angle shift

The $\Delta\theta$ shift during the electrodeposition was simulated using Fresnel reflectivity calculation [35]. The surface roughness "region" on the gold surface was modeled as a layer mixed of gold, IL, and Co (Fig.1a). The Co electrodeposition system was entirely modeled as a four-layer structure composed of prism/Au film/mixed layer/IL

京都大学 KYOTO UNIVERSITY
A Self-archived copy in
Kyoto University Research Information Repository
https://repository.kulib.kyoto-u.ac.jp
京都大学学術情報リポジトリ KURENAI 紅 Kyoto University Research Information Repository

(Fig. 1a). The surface roughness change during electrodeposition was incorporated by two parameters; the Co film thickness deposited in “valleys” (concave parts) and “peaks” (convex parts) on the surface are defined as d_v and d_p, respectively (Fig. 1b). The refractive index of the mixed layer, n_{mix}, was estimated by Bruggeman's effective medium approximation, Eq 1.

$$\sum_{i} f_i \frac{{n_i}^2 - {n_{mix}}^2}{{n_i}^2 + 2{n_{mix}}^2} = 0 \qquad (1)$$

where n_i is the refractive index, f_i is the volume fraction, and i is either Au, Co, or IL. The values of refractive indices at 670 nm are $n_{prism} = 1.691$, $n_{Au} = 0.096 + 3.69i$ [39], $n_{Co} = 2.26 + 4.31i$ [40,41], and n_{IL} =1.427 [35]. By using an approximation $f_{Au} + f_{Co} + f_{IL} = 1$, f_i can be obtained from the area ratio in Fig. 1b as follows

$$f_{Au} = \frac{1}{2}\frac{d_{mix,0}}{d_{mix,0} + d_p}$$
$$f_{IL} = \frac{1}{2}\frac{d_{mix,0} + d_p - d_v}{d_{mix,0} + d_p}$$
$$f_{Co} = \frac{1}{2}\frac{d_p + d_v}{d_{mix,0} + d_p}$$

Among the six n_{mix} solutions of Eq 1, we adopted only one solution in which both the real and imaginary parts of the complex are positive.

The SPR angle was evaluated as a reflectivity minimum in the plots of the reflectivity against the angle of incidence at various d_v and d_p to produce a contour map of $\Delta\theta$ depending on them. The surface roughness of the bare gold surface at $f_{Co} = 0$

A Self-archived copy in
Kyoto University Research Information Repository
https://repository.kulib.kyoto-u.ac.jp

($d_{\mathrm{p}} = d_{\mathrm{v}} = 0$) was set to $d_{\mathrm{mix,0}}$, determined by AFM (see above), and the mixed layer thickness d_{mix} for $f_{\mathrm{Co}} > 0$ was defined as $d_{\mathrm{mix}} = d_{\mathrm{mix,0}} + d_{\mathrm{p}}$ (Fig. 1b).

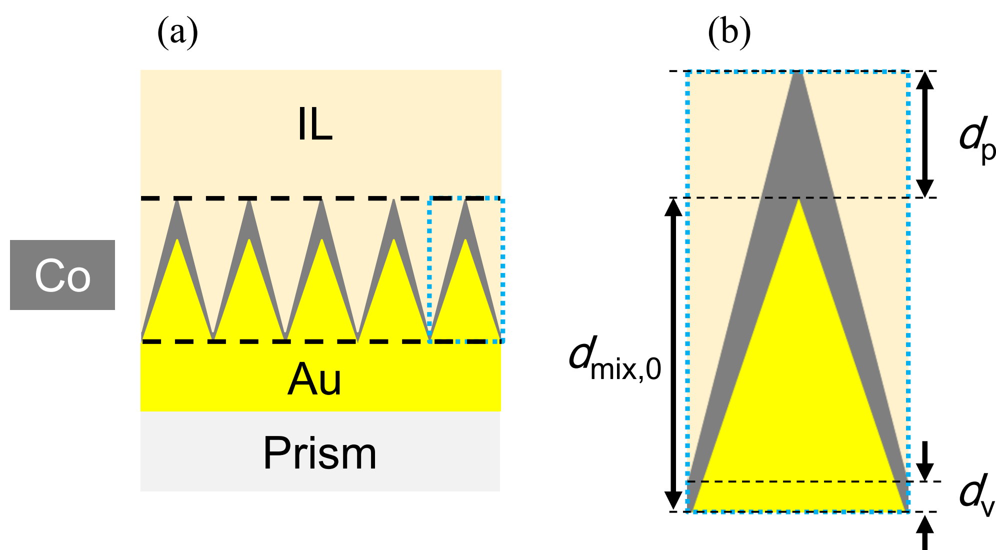

Fig. 1. Schematic diagram of the four-layer model during the cobalt deposition.

3. Results and discussion

3-1. ESPR without additives

Fig. 2 shows the CV and ESPR curves during repeated cathodic deposition and anodic dissolution of Co. A pair of current peaks are discernible in the CVs (Fig. 2a); the negative current peak at −0.68 V in the forward negative scan corresponds to the cathodic deposition of Co, and the positive peak at −0.13 V in the backward positive scan to the anodic dissolution of Co. The peak separation is wide, 0.55 V, indicating that the activation overpotential is high as previously reported [5,7,9–

A Self-archived copy in
Kyoto University Research Information Repository
https://repository.kulib.kyoto-u.ac.jp

11,14,15,17,19,20][21,22,24,25]. ESPR curves (Fig. 2b) show a negative $\Delta\theta$ shift in the negative scans from −0.3 to −0.7 V. This corresponds to the ionic composition change in the EDL, from the anion ($TFSA^-$) rich to cation (C_4mim^+) rich condition when passing the potential of zero charge (E_{pzc}), −0.6 V, as previously confirmed at the C_4mimTFSA/gold interface (see also the red curve in Fig.S2a) [33]. The negative $\Delta\theta$ shift reflects a lower local refractive index for the cation rich ionic layer in the EDL than for the anion rich counterpart, which was revealed by our recent study combining ESPR and molecular dynamics simulation [42]. After the negative shift, $\Delta\theta$ switched to a positive shift at potentials where the cathodic deposition occurs (<−0.7 V). In the positive scan, $\Delta\theta$ still shows a positive shift at the deposition potentials and then becomes constant before Co anodic dissolution starts at −0.2 V. During the anodic dissolution occurs at around −0.1 V, $\Delta\theta$ negatively shifts. After that, $\Delta\theta$ gradually shifts positively caused by slow relaxation of the EDL structure (Fig.S2a), which is prominent not in the negative scan but in the positive scan [33]. This behavior of ESPR curves as well as CVs do not change much with repeated 8 potential scans. The positive $\Delta\theta$ shift originating from Co cathodic deposition ($\Delta\Delta\theta_{dep}$) was +140 mdeg (−20−(−160)), independent of the scan. This scan independence of $\Delta\Delta\theta_{dep}$ is in stark contrast to the previous Cu electrodeposition case, where $\Delta\Delta\theta_{dep}$ for Cu electrodeposition decreased as the scan was repeated [35]. This was attributed to the slow alloying of Cu with Au at room temperature with an atomistic layer on the gold surface, which induces smoothing of the gold surface. Since Co does not form an alloy with Au [43], it is reasonable that we observed no $\Delta\Delta\theta_{dep}$ change during repeated Co electrodeposition in the present study, which suggests that the surface roughness did not change. In fact, ex-situ AFM

京都大学 KYOTO UNIVERSITY
A Self-archived copy in
Kyoto University Research Information Repository
https://repository.kulib.kyoto-u.ac.jp
京都大学学術情報リポジトリ KURENAI 紅 Kyoto University Research Information Repository

observation of the gold surface before and after ESPR measurements showed that the roughness of the gold surface did not change (see below).

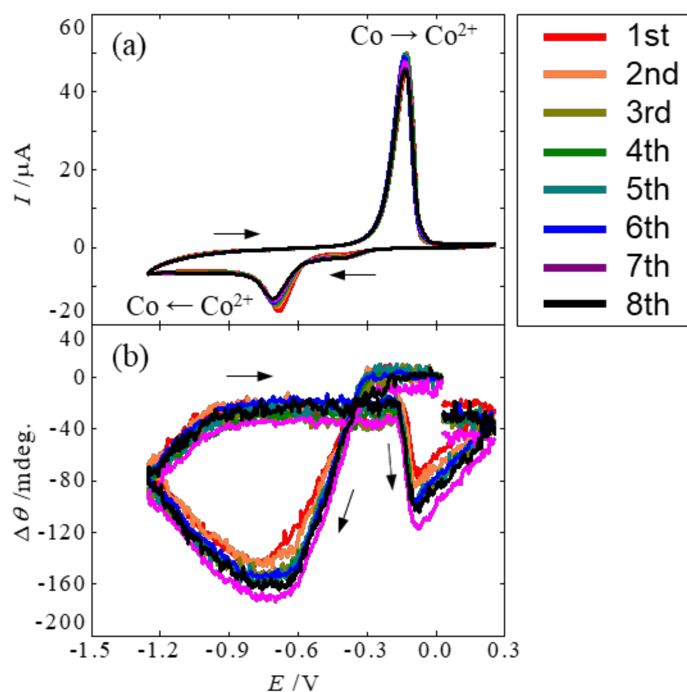

Fig. 2. (a) CVs and (b) ESPR curves at the Au electrode in C_4mimTFSA with 5 mM Co(TFSA)$_2$. Scan rate: 50 mV/s; Start and finish potentials: 0.025 V; First and second reverse potentials: −1.25 V and 0.25 V, respectively.

In order to analyze the ESPR results quantitatively, CV simulations were performed. The details of the simulation are described in Supporting Information. Fig. S1 shows the CV obtained from the simulation (Fig. S1a) and the surface concentrations of Co^{2+}, $c^{s}_{Co^{2+}}$, and Co, Γ_{Co}, on the electrode (Fig. S1b). Since $\Delta\theta$ approximately has a linear relationship with $c^{s}_{Co^{2+}}$ and Γ_{Co} (Eq S12), these surface concentration curves were used to fit the ESPR curves, as shown in Fig. S2. Fig. S2a shows how qualitatively the ESPR curve (black, 1st cycle shown in Fig. 1b) can be explained by the EDL contribution from the ESPR curve without Co (red) [33] that is superimposed on Co film

京都大学 KYOTO UNIVERSITY
A Self-archived copy in
Kyoto University Research Information Repository
https://repository.kulib.kyoto-u.ac.jp
京都大学学術情報リポジトリ KURENAI 紅 Kyoto University Research Information Repository

contribution from the simulated Γ_{Co} (blue). The positive and negative shifts of $\Delta\theta$ with Co deposition and dissolution in the ESPR curve (black in Fig. S2a) detect the increase and decrease of Co surface concentration at the electrode surface. The ESPR curve without Co^{2+} shows a sigmoidal shape, which is attributed to the ionic replacement in the EDL on the gold electrode [33], between the $TFSA^{-}$-rich condition at $E>E_{pzc}$ and the C_4mim^{+}-rich one at $E<E_{pzc}$. Similarly, for the ESPR curve in the presence of Co^{2+}, the $\Delta\theta$ negative shift in the negative scan and the $\Delta\theta$ positive shift in the positive scan is likely to result from the similar ionic composition change in the EDL, because the Co^{2+} concentration is three orders of magnitude lower than that of C_4mim^{+}. The fitting of the EDL and Γ_{Co} curves to the ESPR curve went well for the forward negative scan, as shown in Fig. S2b. The fitting failed in the reverse positive scan, attributed to several reasons such as the E_{pzc} shift due to Co deposition on Au, the slow relaxation of the EDL that is prominent only in the positive scan [33], and the failure of the linearity assumption between $\Delta\theta$ and Γ_{Co} due to the surface roughness change during the Co deposition, the last of which was actually found to occur by the analysis described below.

京都大学 KYOTO UNIVERSITY
A Self-archived copy in
Kyoto University Research Information Repository
https://repository.kulib.kyoto-u.ac.jp
京都大学学術情報リポジトリ KURENAI 紅
Kyoto University Research Information Repository

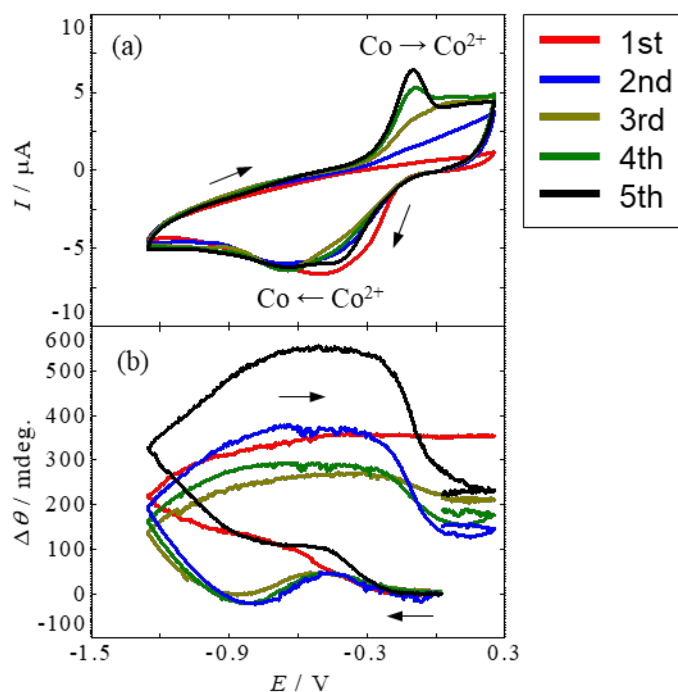

Fig. 3. (a) CVs and (b) ESPR curves at the Au electrode in C_4mimTFSA with 5 mM $Co(TFSA)_2$ and 5 mM TU. Scan rate: 50 mV/s; Start and finish potentials: 0.025 V; First and second reverse potentials: −1.25 V and 0.25 V, respectively.

3-2. ESPR in the presence of TU

Fig. 3 shows the ESPR results for the IL containing 5 mM Co^{2+} and 5 mM TU. In the CV (Fig. 3a), a peak pair was observed as in Fig. 2a, however, the peak separation was relatively narrow and the cathodic current peak was broad. The Co deposition peak was shifted to the positive potential side compared to the case without TU (Fig. 2a). These are the signs of deposition overpotential lowering by the addition of TU, as previously reported [26]. The anodic peak due to Co dissolution was not observed in the first cycle, but became visible with increasing scan cycles. Elemental analysis of the gold surface after ESPR measurement by XPS (Fig. S3) revealed the existence of Co, suggesting that the dissolution of Co was inhibited by the addition of TU. In the ESPR

A Self-archived copy in
Kyoto University Research Information Repository
https://repository.kulib.kyoto-u.ac.jp

(Fig. 3b), positive and negative $\Delta\theta$ shifts were observed due to Co deposition and dissolution, respectively, with a minor contribution of EDL structure change. The $\Delta\Delta\theta_{dep}$ due to Co deposition increased with repeated scans. The $\Delta\Delta\theta_{dep}$ values are larger than those in the case without TU whereas the amount of Co deposition, estimated from the oxidation peak area, is apparently lower. This contradiction at a glance, however, can be explained by the significant contribution of the surface roughness in the positive $\Delta\theta$ shift. Ex-situ AFM observation of the gold surface after ESPR measurement actually confirmed that the surface roughness indeed increased (see below).

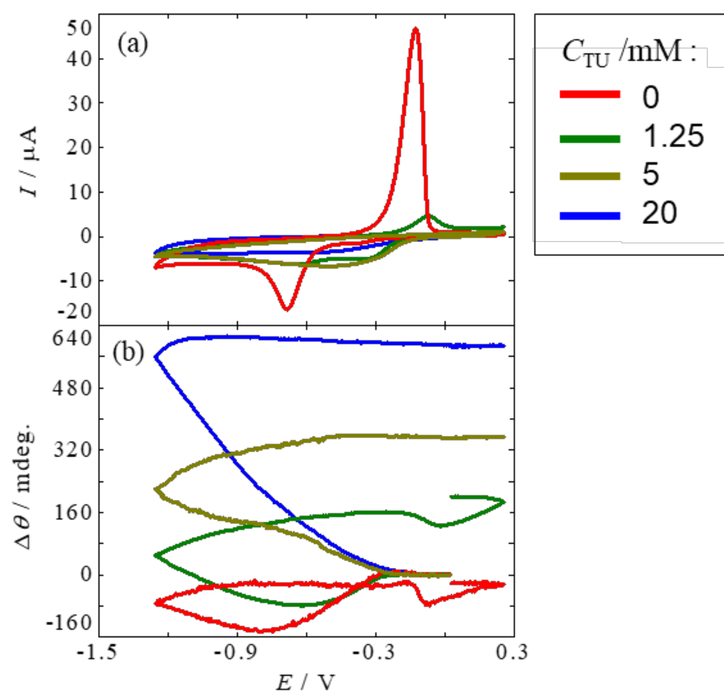

Fig. 4. (a) CVs and (b) ESPR curves at the Au electrode in C_4mimTFSA with 5 mM $Co(TFSA)_2$ and TU. The red, green, yellow, and blue lines show the results at TU concentrations of 0, 1.25, 5, and 20 mM, respectively. Scan rate: 50 mV/s; Start and finish potentials: 0.025 V; First and second reverse potentials: −1.25 V and 0.25 V, respectively.

京都大学 KYOTO UNIVERSITY
A Self-archived copy in
Kyoto University Research Information Repository
https://repository.kulib.kyoto-u.ac.jp
京都大学学術情報リポジトリ KURENAI 紅 Kyoto University Research Information Repository

The results at several concentrations of TU are shown in Fig. 4. Each curve is at the first scan cycle of the measurement among 8 cycles of the potential scan. Even at a low concentration of 1.25 mM, the addition of TU lowered the overpotential of the electrodeposition. At higher TU concentrations, the amount of Co deposition was smaller, but the $\Delta\Delta\theta_{dep}$ was larger. This is due to the large surface roughness of the Co electrodeposited film caused by the addition of TU. It is known that the addition of TU promotes the dissolution of gold [44], and the surface roughness of the Co film will be affected by the surface roughening of the underlying gold. No anodic dissolution of Co was observed at the TU preparation concentrations of 20 and 5 mM, and no negative $\Delta\theta$ shift due to Co dissolution was observed in the ESPR curve. At 5 mM, the anodic dissolution peak (Fig. 3a) and $\Delta\theta$ negative shift (Fig. 3b) were gradually observed after repeated cycles. When the TU concentration was 1.25 mM, the CV and ESPR curves showed a response due to the anodic dissolution of Co, although the response was smaller than that without TU. The anodic dissolution of Co is likely to be inhibited by TU, because the anodic dissolution peak became visible only when the TU concentration was low.

京都大学 KYOTO UNIVERSITY
A Self-archived copy in
Kyoto University Research Information Repository
https://repository.kulib.kyoto-u.ac.jp
京都大学学術情報リポジトリ KURENAI 紅 Kyoto University Research Information Repository

3-3. ESPR in the presence of CM

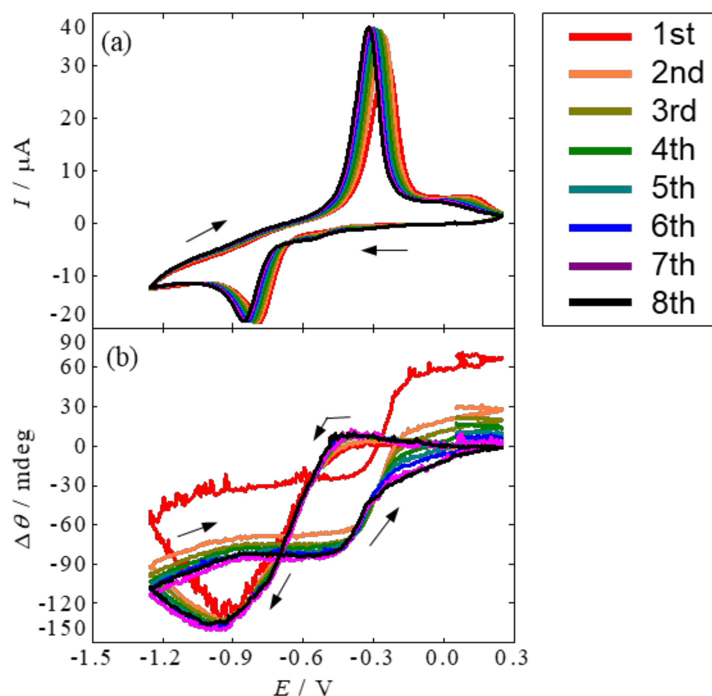

Fig. 5. (a) CVs and (b) ESPR curves at the Au electrode in C_4mimTFSA with 5 mM Co$(TFSA)_2$ and 5 mM CM. Scan rate: 50 mV/s; Start and finish potentials: 0.025 V; First and second reverse potentials: −1.25 V and 0.25 V, respectively.

The results for CM, another leveling additive, are shown in Fig. 5. The CVs (Fig. 5a) show a pair of current peaks as in the above cases, corresponding to the cathodic deposition and anodic dissolution of Co. On the other hand, in the ESPR curve (Fig. 5b), the $\Delta\Delta\theta_{dep}$ associated with Co deposition was smaller: 100 mdeg at the 1st cycle and 50 mdeg at the subsequent cycles compared with 140 mdeg without additives (Fig. 2b), suggesting that the Co film surface was smoothed by CM. This is in contrast to the large $\Delta\Delta\theta_{dep}$ observed when TU was added (see above). During the anodic dissolution of Co, $\Delta\theta$ was positively shifted, which is opposite to the behaviors without additives (Fig. 2b)

京都大学 KYOTO UNIVERSITY
A Self-archived copy in
Kyoto University Research Information Repository
https://repository.kulib.kyoto-u.ac.jp
京都大学学術情報リポジトリ KURENAI 紅 Kyoto University Research Information Repository

and with TU (Fig. 3b). This suggests an increase in the surface roughness of the Co film during the dissolution process. Fig.S2c shows the fitting result of CV simulation (Fig. S1c,d) to the experimental ESPR curve as is the case without additives. Among the parameters a and b in Eq S12, the former is from the diffusion layer of Co^{2+} and the parameter a should be the same for the cases with and without CM. Therefore, the parameter a was constrained to be the same regardless of the presence and absence of CM. The latter parameter, b, comes from the contributions from the deposited metal film and surface roughness change, which cannot be separated because it is the metal film itself to change the surface roughness. However, we can evaluate the parameter b as a measure of how the surface roughness changes during the metal deposition. An increase (decrease) in the surface roughness in the deposition process will result in a larger (smaller) b value. The best fit parameters are: $a = 9\ \mathrm{mdeg/(mol\ m^{-3})}$ and $b = 23\ \mathrm{mdeg/(10^{-5}\ mol\ m^{-2})}$ in the presence of CM whereas $b = 42\ \mathrm{mdeg/(10^{-5}\ mol\ m^{-2})}$ in the absence of CM. The smaller b value when CM is added is likely due to the smoother surface of the electrodeposited Co film, indicating that CM actually works as a leveler even in the initial process of the Co electrodeposition.

京都大学 KYOTO UNIVERSITY
A Self-archived copy in
Kyoto University Research Information Repository
https://repository.kulib.kyoto-u.ac.jp
京都大学学術情報リポジトリ KURENAI 紅 Kyoto University Research Information Repository

3-4. Ex-situ AFM observation of gold surface

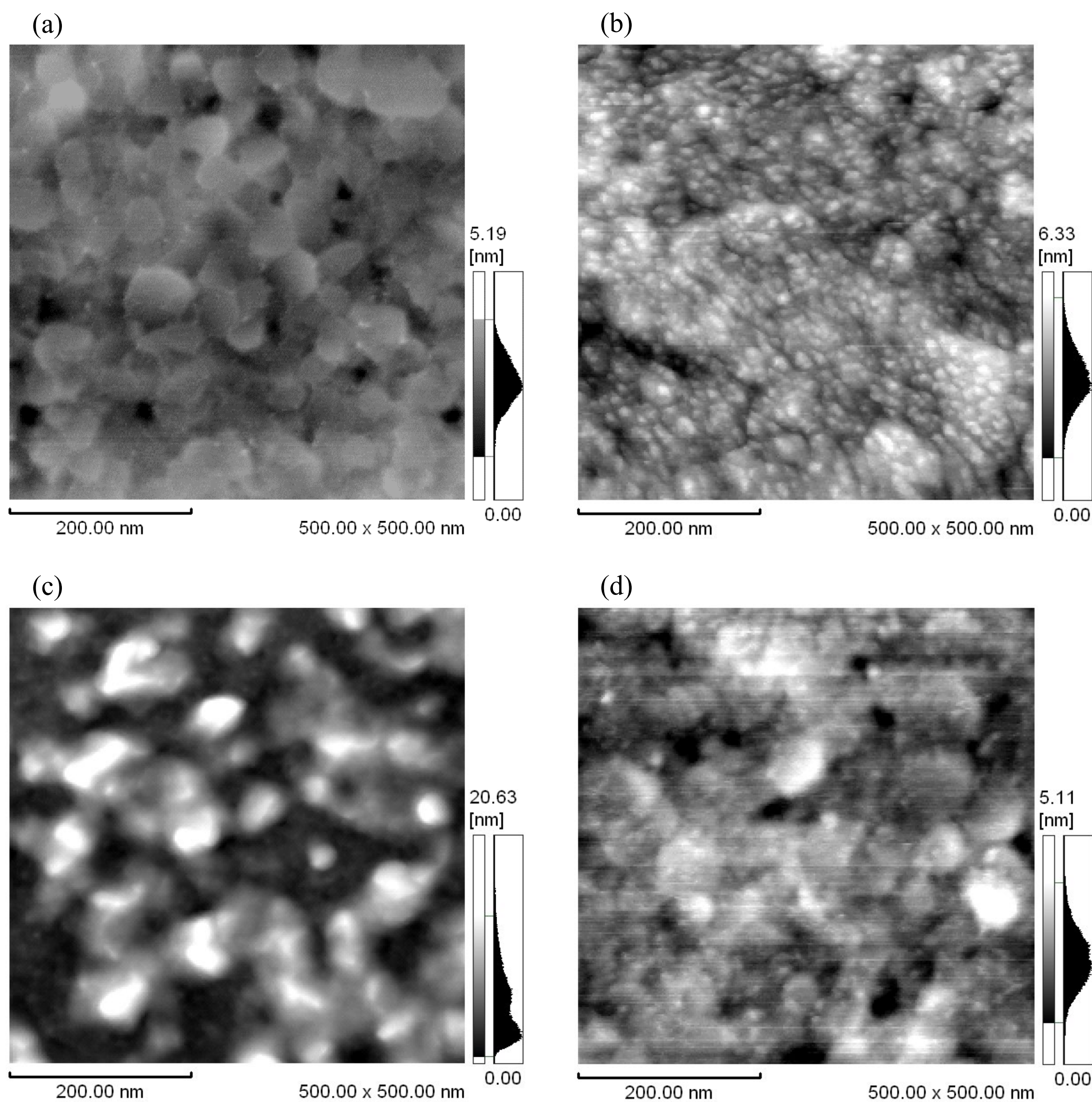

Fig. 6. Ex-situ AFM images of the gold surface (a) before and (b-d) after ESPR measurements in C_4mimTFSA with 5 mM $Co(TFSA)_2$; (b) without additives, (c) with 5 mM TU, and (d) with 5 mM CM.

A Self-archived copy in
Kyoto University Research Information Repository
https://repository.kulib.kyoto-u.ac.jp

Table 1. Ex-situ AFM results.

		R_q (nm)	$d_{mix,0}$ [a)] (nm)
Before ESPR		0.9	1.1±0.3
After ESPR	without additives	1.1	1.3±0.3
	with TU (5 mM)	5.2	6.1±1.5
	with CM (5 mM)	1.1	1.3±0.3

[a)] Estimated using the relation $d_{\mathrm{mix,0}} = (1.175 \pm 0.285)R_{\mathrm{q}}$ [40,41].

The AFM images of the gold surface before and after ESPR measurements are shown in Fig. 6. The root-mean-square roughness (R_q) and the calculated roughness layer thickness ($d_{mix,0}$) for all the images in Fig. 6 are listed in Table 1. Fig. 6a shows the image before ESPR measurement. Gold grains with a lateral size of several tens nm and with a flat top were observed. Fig. 6b shows the surface after ESPR measurement with the IL without additives (Fig. 2). The gold grains became finer but the R_q evaluated from the image was almost unchanged before and after the ESPR measurement. This is consistent with the ESPR results (Fig. 2b), which show no cycle dependence of $\Delta\Delta\theta_{dep}$. Fig. 6c shows the surface after the ESPR measurement with C_{TU} = 5 mM (Fig. 3). The shape of the gold grains is hardly visible and the surface roughness apparently increased, which is actually evaluated as a greater R_q value (Table 1). This surface roughness increase is consistent with the anomalous $\Delta\theta$ positive shift in the ESPR curves (Fig. 3b). Fig. 6d shows the surface after the ESPR measurement with C_{CM} = 5 mM (Fig. 5), where gold grains can be seen with fine particles on them. The R_q value indicates that the roughness of the gold surface did not change (Table 1). Therefore, the reason why $\Delta\Delta\theta_{dep}$ is smaller when CM is added is probably that the surface roughness of the electrodeposited film becomes smaller, not because of the gold surface. The surface

A Self-archived copy in
Kyoto University Research Information Repository
https://repository.kulib.kyoto-u.ac.jp

morphology change observed in Fig. 6b,d may be due to the miniaturization of gold particles facilitated by Co deposition/dissolution processes. Previous in-situ STM studies on the Co electrodeposition in ILs on the Au(111) surface revealed that the anodic dissolution of deposited Co accompanies pit formation at the Au(111) surface [14,15,18]. This atomic-scale "roughening" will occur even at the polycrystalline gold surface. In the present study, the 8 cycles of the Co deposition/dissolution processes are likely to make such a change in the surface morphology accumulated and visualized in the ex-situ AFM images (Fig. 6b,d) laterally, although the surface roughness change in the vertical direction evaluated as R_q is still marginal (Table 1). Regarding the possibility of residual Co, the current efficiency of anodic dissolution was evaluated by integrating the CV, based on an assumption that the cathodic and anodic currents were due entirely to Co deposition and dissolution, respectively. In the no-additive condition (Fig. 2a), the current efficiency was 77 %, which corresponds to the thickness of Co remaining on the gold surface being 0.2 nm on average. For the CM addition case (Fig. 5a), the current efficiency was 65 % and the average thickness of the remaining Co was 0.4 nm. The current efficiency decreased probably because of the reductive decomposition of CM, which is the leveling mechanism.

京都大学 KYOTO UNIVERSITY
A Self-archived copy in
Kyoto University Research Information Repository
https://repository.kulib.kyoto-u.ac.jp
京都大学学術情報リポジトリ KURENAI 紅 Kyoto University Research Information Repository

3-5. Fresnel reflectivity simulation

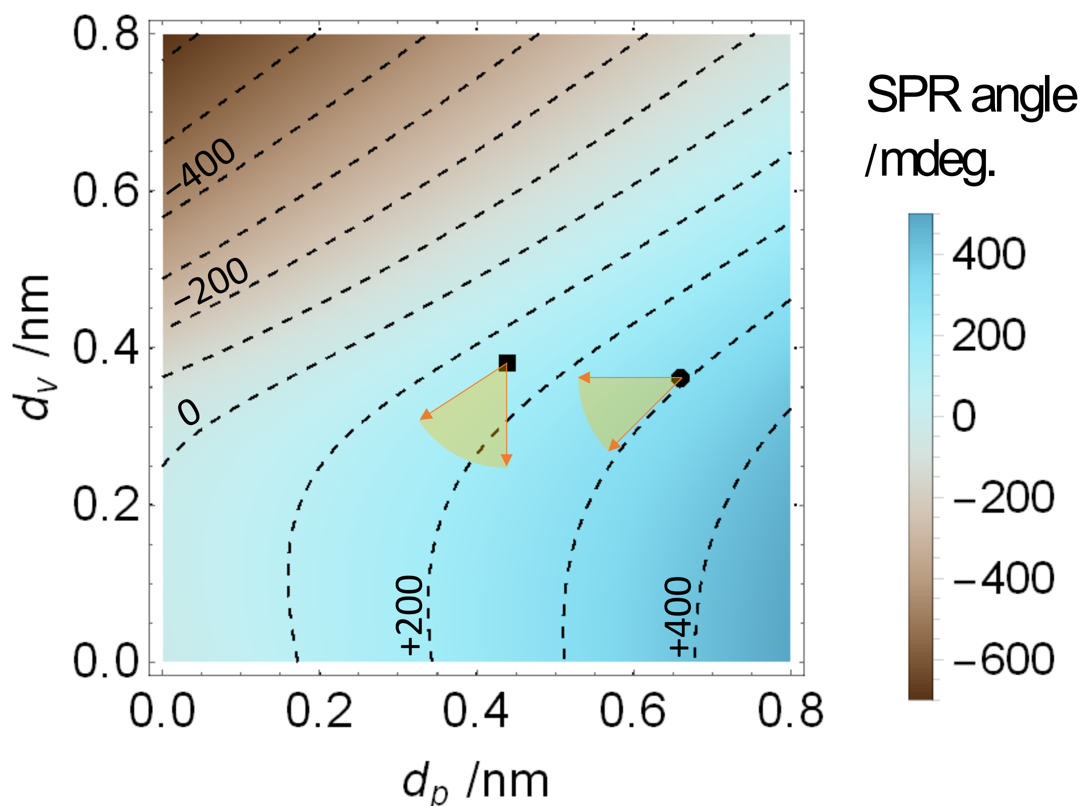

Fig. 7. Contour map for the Δθ shift against the cobalt deposition ($\Delta\Delta\theta_{\mathrm{dep}}$ = 0 at (d_{p}, d_{v}) = (0, 0)). The solid square and circle represent the surface conditions of the Co film formed with and without CM, respectively. The orange fan-shaped arrow regions show possible directions to which the anodic dissolution of the Co film proceeds, which is determined by positive and negative Δθ shift with and without CM, respectively, and a constraint of negative directions along both the d_{p} and d_{v} axes for the anodic dissolution.

The $\Delta\Delta\theta_{\mathrm{dep}}$ during Co deposition depends on whether CM was present or not (Fig. 2b, 5b), whereas the surface roughness of the gold substrate after the ESPR measurements did not change (Fig. 6, Table 1). This is attributable to the difference in surface roughness of the deposited film, not that of the gold substrate. In order to investigate the dependence of $\Delta\Delta\theta_{\mathrm{dep}}$ on the two surface roughnesses, Fresnel reflectivity simulations

京都大学 KYOTO UNIVERSITY
A Self-archived copy in
Kyoto University Research Information Repository
https://repository.kulib.kyoto-u.ac.jp
京都大学学術情報リポジトリ KURENAI 紅 Kyoto University Research Information Repository

were performed. Fig. 7 shows the $\Delta\theta$ shift depending on two variables, d_p and d_v (see Fig.1b for their definitions). The relationship $d_p > d_v$ ($d_p < d_v$) corresponds to the roughened (smoothed) Co film surface compared with the gold substrate. The two variables for the Co film were evaluated as follows. The average thickness of deposited Co film, d_{Co}, has a relationship with the two variables, as shown in Fig. 1:

$$d_{Co} = \frac{d_p + d_v}{2} \tag{4}$$

d_{Co} was estimated using the following equation

$$d_{Co} = \frac{q m_{Co}}{2F\rho S} \tag{3}$$

where m_{Co} is the molar mass of Co (58.9 g mol^{-1}), ρ is the Co density (8.90 g cm^{-3}), S is the electrode surface (0.071 cm^2), F is the Faraday constant, and q is the charge by integrating the current peak of Co anodic dissolution. d_{Co} was evaluated to be 0.51 nm without CM and 0.41 nm with CM. To find the points in the contour map in Fig.7 that represent the surface roughness condition of the Co film, the d_{Co} values and the relationship between d_p and d_v in Eq 4 were combined with $b\Gamma_{Co,max}$, which is the contribution of the Co film to $\Delta\theta$. Here the b values are 42 and 23 mdeg/(10^{-5} mol m^{-2}) from the fitting (Fig.S2b,c) and the $\Gamma_{Co,max}$ values are 7.1 and 6.3 (10^{-5} mol m^{-2}) from the CV simulations (Fig.S1b,d) without and with CM, respectively. The found points are: (d_p, d_v) = (0.66, 0.36) [nm] without CM, and (d_p, d_v) = (0.44, 0.38) [nm] with CM (Fig.7). Both have the relation $d_p > d_v$, indicating that the

A Self-archived copy in
Kyoto University Research Information Repository
https://repository.kulib.kyoto-u.ac.jp

surface roughness of the deposited film increases, compared to the gold surface condition before the deposition, i.e., the surface roughness of the gold electrode. However, the extent to roughen the surface is lower with the CM case. The extent may be quantified as a normalized quantity, $(d_{\mathrm{p}} - d_{\mathrm{v}})/(d_{\mathrm{p}} + d_{\mathrm{v}})$, which is in the range between -1 and 1 with a more positive value corresponding to a more roughened surface. The values are 0.30 and 0.07 without and with CM, respectively, which quantitatively confirms that CM works as a leveler. This illustrates that the smoothing of the electrodeposition film by the addition of CM can be detected even in the very beginning stage of electrodeposition in-situ by ESPR with high sensitivity.

In the anodic dissolution of Co, $d_{\mathrm{p}} + d_{\mathrm{v}}$ should decrease, however, the $\Delta\theta$ trend was different in the presence and absence of CM; $\Delta\theta$ shifted negatively without CM but positively with CM. This indicates that, during Co anodic dissolution, the surface condition location in the contour map proceeds in the direction of decreasing $d_{\mathrm{p}} - d_{\mathrm{v}}$ without CM and increasing $d_{\mathrm{p}} - d_{\mathrm{v}}$ with CM (orange fan-shaped arrow regions in Fig. 7). In other words, the Co film was anodically dissolved in the direction of decreasing the surface roughness of the film without additives, while in the direction of increasing the surface roughness when CM was added.

4. Conclusions

ESPR measurements in the initial process of the Co electrodeposition showed that Co deposition, EDL composition change, and surface roughness change can be simultaneously detected. In the case without additives, the roughness of the gold surface did not change due to repeated Co deposition and dissolution, in stark contrast to the Cu deposition case [35].

A Self-archived copy in
Kyoto University Research Information Repository
https://repository.kulib.kyoto-u.ac.jp

In the presence of leveling additives, the situation significantly changed. When TU was added, $\Delta\Delta\theta_{dep}$ increased with each cycle during Co deposition, due to the roughening of the gold surface by TU assisted gold dissolution. On the other hand, when CM was added, the $\Delta\Delta\theta_{dep}$ during the Co deposition became smaller than the non-additive case, due to the fact that the surface roughness of the Co deposited film was smaller and CM contributed to smooth the electrodeposited film. The Fresnel reflection simulation suggested that a positive shift of $\Delta\theta$ during the Co dissolution process in the presence of CM was attributed to the increase in the surface roughness of the electrodeposited film, a process opposite to the smoothing during the deposition.

Acknowledgements

We acknowledge Dr. Yuki Kitazumi for the AFM measurements. This work was partly supported by JSPS KAKENHI (Nos. 18K05171 and 21H02046), Kato Foundation for Promotion of Science (KJ-2819), and Izumi Science and Technology Foundation (2020-J-071).

References

[1] H. Sun, G. Zhu, X. Xu, M. Liao, Y.Y. Li, M. Angell, M. Gu, Y. Zhu, W.H. Hung, J. Li, Y. Kuang, Y. Meng, M.C. Lin, H. Peng, H. Dai, A safe and non-flammable sodium metal battery based on an ionic liquid electrolyte, Nat. Commun. 10 (2019) 1–11. https://doi.org/10.1038/s41467-019-11102-2.

[2] K. Liu, Z. Wang, L. Shi, S. Jungsuttiwong, S. Yuan, Ionic liquids for high performance lithium metal batteries, J. Energy Chem. 59 (2021) 320–333. https://doi.org/10.1016/j.jechem.2020.11.017.

[3] A.P. Abbott, K.J. McKenzie, Application of ionic liquids to the electrodeposition of metals, Phys. Chem. Chem. Phys. 8 (2006) 4265–4279. https://doi.org/10.1039/b607329h.

京都大学 KYOTO UNIVERSITY

A Self-archived copy in
Kyoto University Research Information Repository
https://repository.kulib.kyoto-u.ac.jp

京都大学学術情報リポジトリ KURENAI 紅 Kyoto University Research Information Repository

[4] F. Endres, S. Zein El Abedin, Air and water stable ionic liquids in physical chemistry, Phys. Chem. Chem. Phys. 8 (2006) 2101–2116. https://doi.org/10.1039/b600519p.

[5] C.L. Hussey, T.M. Laher, Electrochemical and spectroscopic studies of cobalt(II) in molten aluminum chloride-n-butylpyridinium chloride, Inorg. Chem. 20 (1981) 4201–4206. https://doi.org/10.1021/ic50226a034.

[6] R.T. Carlin, P.C. Trulove, H.C. De Long, Electrodeposition of Cobalt-Aluminum Alloys from Room Temperature Chloroaluminate Molten Salt, J. Electrochem. Soc. 143 (1996) 2747–2758. https://doi.org/10.1149/1.1837102.

[7] J.A. Mitchell, W.R. Pitner, C.L. Hussey, G.R. Stafford, R.T. Carlin, P.C. Trulove, H.C. De Long, Electrodeposition of Cobalt and Cobalt-Aluminum Alloys from a Room Temperature Chloroaluminate Molten Salt, J. Electrochem. Soc. 143 (1996) 3448–3455. https://doi.org/10.1149/1.1837235.

[8] N. Koura, T. Endo, Y. Idemoto, The electrodeposition of amorphous Co-Zn alloy from ambient temperature molten salt electrolytes, J. Non. Cryst. Solids. 205–207 (1996) 650–655. https://doi.org/10.1016/S0022-3093(96)00289-X.

[9] M.R. Ali, A. Nishikata, T. Tsuru, Electrodeposition of Co-Al alloys of different composition from the AlCl3-BPC-CoCl2 room temperature molten salt, Electrochim. Acta. 42 (1997) 1819–1828. https://doi.org/10.1016/S0013-4686(96)00382-9.

[10] R.T. Carlin, H.C. De Long, J. Fuller, P.C. Trulove, Microelectrode Evaluation of Transition Metal-Aluminum Alloy Electrodepositions in Chloroaluminate Ionic Liquids, J. Electrochem. Soc. 145 (1998) 1598–1607. https://doi.org/10.1149/1.1838524.

[11] P.-Y. Chen, I.-W. Sun, Electrodeposition of cobalt and zinc-cobalt alloys from a lewis acidic zinc chloride-1-ethyl-3-methylimidazolium chloride molten salt, Electrochim. Acta. 46 (2001) 1169–1177. https://doi.org/10.1016/S0013-4686(00)00703-9.

[12] F. Endres, Ionic liquids: Solvents for the electrodeposition of metals and semiconductors, ChemPhysChem. 3 (2002) 144–154. https://doi.org/10.1002/1439-7641(20020215)3:2<144::aid-cphc144>3.0.co;2-%23.

[13] H.-Y. Hsu, C.-C. Yang, Conductivity, Electrodeposition and Magnetic Property of Cobalt(II) and Dysprosium Chloride in Zinc Chloride-1-Ethyl-3-Methylimidazolium Chloride Room Temperature Molten Salt, Z. Naturforsch. B. 58 (2003) 139–146. https://doi.org/10.1515/znb-2003-0120.

[14] C.A. Zell, W. Freyland, In situ STM and STS study of Co and Co-Al alloy electrodeposition from an ionic liquid, Langmuir. 19 (2003) 7445–7450. https://doi.org/10.1021/la030031i.

[15] W. Freyland, C.A. Zell, S. Zein El Abedin, F. Endres, Nanoscale electrodeposition of metals and semiconductors from ionic liquids, Electrochim. Acta. 48 (2003) 3053–3061. https://doi.org/10.1016/S0013-4686(03)00378-5.

A Self-archived copy in
Kyoto University Research Information Repository
https://repository.kulib.kyoto-u.ac.jp

[16] C.-C. Yang, T.-H. Wu, M.-F. Shu, Magnetic Films of Cobalt/Aluminum Electrodeposited from the Room Temperature Molten Salts AlCl3-BPC-CoCl3, Z. Naturforsch. B. 59 (2004) 519–524. https://doi.org/10.1515/znb-2004-0505.

[17] R. Fukui, Y. Katayama, T. Miura, Electrodeposition of cobalt from a hydrophobic room-temperature molten salt system, Electrochemistry. 73 (2005) 567–569. https://doi.org/10.5796/electrochemistry.73.567.

[18] L.G. Lin, J.W. Yan, Y. Wang, Y.C. Fu, B.W. Mao, An in situ STM study of cobalt electrodeposition on Au(111) in BMIBF4 ionic liquid, J. Exp. Nanosci. 1 (2006) 269–278. https://doi.org/10.1080/17458080601009643.

[19] S. Schaltin, P. Nockemann, B. Thijs, K. Binnemans, J. Fransaer, Influence of the anion on the electrodeposition of cobalt from imidazolium ionic liquids, Electrochem. Solid-State Lett. 10 (2007) D104–D107. https://doi.org/10.1149/1.2760185.

[20] Y. Katayama, R. Fukui, T. Miura, Electrodeposition of Cobalt from an Imide-Type Room-Temperature Ionic Liquid, ECS Trans. 3 (2007) 287–295. https://doi.org/10.1149/1.2798672.

[21] C. Su, M. An, P. Yang, H. Gu, X. Guo, Electrochemical behavior of cobalt from 1-butyl-3-methylimidazolium tetrafluoroborate ionic liquid, Appl. Surf. Sci. 256 (2010) 4888–4893. https://doi.org/10.1016/j.apsusc.2010.02.087.

[22] R. Fukui, Y. Katayama, T. Miura, The effect of organic additives in electrodeposition of Co from an amide-type ionic liquid, Electrochim. Acta. 56 (2011) 1190–1196. https://doi.org/10.1016/j.electacta.2010.10.074.

[23] M. Tułodziecki, J.M. Tarascon, P.L. Taberna, C. Guéry, Importance of the double layer structure in the electrochemical deposition of Co from soluble Co2+ - Based precursors in Ionic Liquid media, Electrochim. Acta. 134 (2014) 55–66. https://doi.org/10.1016/j.electacta.2014.03.042.

[24] X. He, Z. Sun, Q. Zou, L. Wu, J. Jiang, Electrochemical Behavior of Co(II) Reduction for Preparing Nanocrystalline Co Catalyst for Hydrogen Evolution Reaction from 1-ethyl-3-methylimidazolium Bisulfate and Ethylene Glycol System, J. Electrochem. Soc. 166 (2019) D57–D64. https://doi.org/10.1149/2.0981902jes.

[25] K. Motobayashi, Y. Shibamura, K. Ikeda, Origin of a High Overpotential of Co Electrodeposition in a Room-Temperature Ionic Liquid, J. Phys. Chem. Lett. 11 (2020) 8697–8702. https://doi.org/10.1021/acs.jpclett.0c02605.

[26] Y. Yasui, Y. Kitazumi, R. Ishimatsu, N. Nishi, T. Kakiuchi, Ultraslow response of interfacial tension to the change in the phase-boundary potential at the interface between water and a room-temperature ionic liquid, trioctylmethylammonium bis(nonafluorobutanesulfonyl)amide, J. Phys. Chem. B. 113 (2009). https://doi.org/10.1021/jp9006312.

[27] N. Nishi, Y. Hirano, T. Motokawa, T. Kakiuchi, Ultraslow relaxation of the structure at the ionic liquid-gold electrode interface to a potential step probed by electrochemical surface plasmon

A Self-archived copy in
Kyoto University Research Information Repository
https://repository.kulib.kyoto-u.ac.jp

resonance measurements: Asymmetry of the relaxation time to the potential-step direction, Phys. Chem. Chem. Phys. 15 (2013) 11615–11619. https://doi.org/10.1039/c3cp51463c.

[28] T. Mimani, S.M. Mayanna, Thermodynamics of Adsorption of Brighteners on Polarized Nickel from Watts Bath Solution, J. Electrochem. Soc. 140 (1993) 984–988. https://doi.org/10.1149/1.2056240.

[29] S. Goldbach, R. De Kermadec, F. Lapicque, Electrodeposition of Ni-Co alloys from sulfamate baths, J. Appl. Electrochem. 30 (2000) 277–284. https://doi.org/10.1023/A:1003938310824.

[30] C. Cheng, A.C. West, Nickel Deposition in the Presence of Coumarin: An Electrochemical Impedance Spectroscopy Study, J. Electrochem. Soc. 144 (1997) 3050–3056. https://doi.org/10.1149/1.1837957.

[31] C. Madore, D. Landolt, Blocking Inhibitors in Cathodic Leveling: II. Experimental Investigation, J. Electrochem. Soc. 143 (1996) 3936–3943. https://doi.org/10.1149/1.1837319.

[32] C. Madore, M. Matlosz, D. Landolt, Blocking Inhibitors in Cathodic Leveling: I. Theoretical Analysis, J. Electrochem. Soc. 143 (1996) 3927–3936. https://doi.org/10.1149/1.1837318.

[33] S. Zhang, N. Nishi, T. Sakka, Electrochemical surface plasmon resonance measurements of camel-shaped static capacitance and slow dynamics of electric double layer structure at the ionic liquid/electrode interface, J. Chem. Phys. 153 (2020) 044707. https://doi.org/10.1063/5.0011671.

[34] N. Nishi, Y. Ikeda, T. Sakka, Electrochemical surface plasmon resonance as a probe of redox reactions at the ionic liquid|gold interface, J. Electroanal. Chem. 817 (2018) 210–216. https://doi.org/10.1016/j.jelechem.2018.03.067.

[35] K. Ezawa, N. Nishi, T. Sakka, In-situ electrochemical SPR study of gold surface smoothing by repetitive cathodic deposition and anodic dissolution of copper in an ionic liquid, J. Electroanal. Chem. 877 (2020) 114611. https://doi.org/10.1016/j.jelechem.2020.114611.

[36] S. Makino, Y. Kitazumi, N. Nishi, T. Kakiuchi, Charging current probing of the slow relaxation of the ionic liquid double layer at the Pt electrode, Electrochem. Commun. 13 (2011) 1365–1368. https://doi.org/10.1016/j.elecom.2011.08.009.

[37] P. Petrik, L.P. Biró, M. Fried, T. Lohner, R. Berger, C. Schneider, J. Gyulai, H. Ryssel, Comparative study of surface roughness measured on polysilicon using spectroscopic ellipsometry and atomic force microscopy, Thin Solid Films. 315 (1998) 186–191. https://doi.org/10.1016/S0040-6090(97)00349-0.

[38] Y. Liu, J. Qiu, L. Liu, Applicability of the effective medium approximation in the ellipsometry of randomly micro-rough solid surfaces, Opt. Express. 26 (2018) 16560. https://doi.org/10.1364/oe.26.016560.

[39] S. Babar, J.H. Weaver, Optical constants of Cu, Ag, and Au revisited, Appl. Opt. 54 (2015) 477. https://doi.org/10.1364/ao.54.000477.

京都大学 KYOTO UNIVERSITY
A Self-archived copy in
Kyoto University Research Information Repository
https://repository.kulib.kyoto-u.ac.jp
京都大学学術情報リポジトリ KURENAI 紅 Kyoto University Research Information Repository

[40] P. B. Johnson, R. W. Christy, P.B. Johnson, R.W. Christy, Optical constants of transition metals, Phys. Rev. B. 9 (1974) 5056–5070.

[41] A.Y.C. Yu, T.M. Donovan, W.E. Spicer, Optical properties of cobalt, Phys. Rev. 167 (1968) 670–673. https://doi.org/10.1103/PhysRev.167.670.

[42] S. Zhang, N. Nishi, S. Katakura, T. Sakka, Evaluation of Static Differential Capacitance at the [C4mim+][TFSA−]/Electrode Interface Using Molecular Dynamics Simulation Combined with Electrochemical Surface Plasmon Resonance Measurements, Phys. Chem. Chem. Phys. in press (2021). https://doi.org/10.1039/d1cp01435h.

[43] H. Okamoto, T.B. Massalski, T. Nishizawa, M. Hasebe, The Au-Co (Gold-Cobalt) system, Bull. Alloy Phase Diagrams. 6 (1985) 449–454. https://doi.org/10.1007/BF02869509.

[44] J. Li, J.D. Miller, A review of gold leaching in acid thiourea solutions, Miner. Process. Extr. Metall. Rev. 27 (2006) 177–214. https://doi.org/10.1080/08827500500339315.